

On the dynamics of mortality and the ephemeral nature of mammalian megafauna

Taran Rallings^{1,*}, Christopher P Kempes², Justin D. Yeakel^{1,*}

¹*School of Natural Sciences, University of California Merced*

²*Santa Fe Institute*

*Corresponding author: trallings@ucmerced.edu; jyeakel@ucmerced.edu

Energy flow through consumer-resource interactions is largely constrained by body size. Allometric relationships govern the dynamics of populations by impacting rates of reproduction, as well as alternative sources of mortality, which have differential impacts on smaller to larger organisms. Here we derive the timescales associated with four alternative sources of mortality for terrestrial mammals: mortality from starvation, mortality associated with aging, mortality from consumption by predators, and mortality introduced by subsidized harvest. The incorporation of these allometric relationships into a minimal consumer-resource model illuminates central constraints that may contribute to the structure of mammalian communities. Our framework reveals that while starvation largely impacts smaller-bodied species, the allometry of senescence is expected to be more difficult to observe. In contrast, external predation and subsidized harvest primarily influence larger-bodied species. The inclusion of predation mortality reveals mass thresholds for mammalian herbivores, where dynamic instabilities may limit the feasibility of megafaunal populations. Moreover, we show how these thresholds vary with alternative predator-prey mass ratios, a relationship that is little understood within terrestrial systems. Finally, we use our framework to predict the harvest pressure required to induce mass-specific extinctions, which closely align with previous estimates of megafaunal exploitation in both paleontological and historical contexts.

I. INTRODUCTION

Consumer-resource interactions are the fundamental unit from which complex food webs arise [1]. In such dynamics, the rates governing transitions of biomass and energy from one species to another are largely determined by body size [2]. Specifically, the allometric relationships between consumer body mass and metabolic rate constrain energetic assimilation [3], storage [4], and growth [5], all of which govern the dynamics of populations [6–9]. Because allometrically-constrained models of population dynamics apply generally across large taxonomic clades, they are useful for examining dynamic constraints that may contribute to community structure across macroevolutionary timescales [9, 10]. Furthermore, examination of community dynamics at these scales enables the investigation of extinct communities where body size distributions were different than those in contemporary ecosystems [11–13].

The dynamics of populations represent an energetic balance between reproduction and mortality [14]. While reproduction is typically predictable from allometric scaling relationships [15], mortality has a variety of forms that do not all scale similarly. Mortality originates from both internal and external drivers, where the former depends on an organism’s internal state to initiate death. For example, senescence and starvation involve physiological states that change with respect to clock time, metabolic rate, and resource depletion [9, 16]. In contrast, external drivers of mortality consist of an outside force that induces death more independently of an organism’s internal state, such as mortality due to natural predation or subsidized anthropogenic harvest. Often mortality occurs through correlations between internal and external drivers, where for example, the starvation

state of prey may alter the success rates of predators [17]. While virtually all primary consumer populations must deal with the effects of resource limitation, aging, and predation, the effects of harvesting are uniquely limited to those species serving as resources for human populations [18].

How do different sources of mortality impact the dynamics of mammalian populations? Here we construct a general consumer-resource framework to examine mammalian herbivore populations as a function of consumer body size M_C , as well as size-dependent vulnerability to different internal and external pressures. Our approach integrates relationships governing specific timescales governing physiology and assimilation from a process-based energetic perspective [5]. Our model is low-dimensional and compact, [cf. 9] but due to its close connection to fundamental energetic mechanism it is also capable of reproducing observed large-scale empirical patterns of mammalian communities. We begin by describing our approach, reproducing key macroecological relationships such as Damuth’s law [19], and then examining how changes to energetic parameters impact these predictions. We then derive timescales associated with four sources of mortality experienced by mammalian consumers: *i*) natural mortality, *ii*) starvation mortality, *iii*) natural predation, and *iv*) subsidized anthropogenic harvest. By examining each source of mortality in turn, our framework illuminates central constraints governing mass-specific behaviors, strategies, and risks experienced by mammalian consumers.

Our results reveal four key insights into the constraints structuring mammalian communities. First, our allometric consumer-resource system accurately captures both the central tendency and variability of Damuth’s law, suggesting that the included vital rates capture mass-

specific dynamics. Second, our results demonstrate that natural and starvation mortality differentially impact small mammals, confirming expectations, and point to why the allometric effects of senescence are difficult to observe in nature. Third, we detail the differences in how mortality from specialist or generalist predators induce population instabilities for large-bodied herbivores. We also show that the body size at which these instabilities occur is dependent on the prevailing predator-prey mass ratio (PPMR). Finally, we evaluate the harvest pressure required to induce mass-specific extinction, and show that our predictions are comparable to estimates of both paleontological and historical exploitation of mammalian megafauna.

II. ALLOMETRIC CONSUMER-RESOURCE MODEL

We model a consumer-resource interaction, where the resource R (g/m^2) grows logistically with intrinsic growth rate α to a carrying capacity k , and declines due to consumption by an herbivore consumer population C (g/m^2) (Eq. 3). Consumed resources govern both consumer somatic maintenance and reproduction. The rate of consumption to fuel somatic maintenance is given by ρ , and is independent of resource density, as these are invariant requirements of the consumer population [9]. In contrast, the rate of consumption to fuel reproduction is proportional to resource density and is given by $\lambda_C(R)/Y_C$, where $\lambda_C(R)$ is the consumer growth rate and Y_C is the consumer yield coefficient, or the grams of consumer produced per gram of resource consumed. As in DeLong & Vasseur [20], the consumer's growth rate $\lambda_C(R)$ follows Michaelis-Menton (Type II) kinetics as a function of the resource density R , where the maximum growth is λ_C^{\max} and the resource half-saturation density is $\hat{k} = k/2$, such that

$$\lambda_C(R) = \lambda_C^{\max} \left(\frac{R}{\hat{k} + R} \right). \quad (1)$$

While the consumer population density grows at rate $\lambda_C(R)$, we assume for now that consumer mortality is a function of both natural mortality μ and starvation $\sigma(R)$, where the rate of starvation,

$$\sigma(R) = \sigma^{\max} \left(1 - \frac{R}{k} \right), \quad (2)$$

increases as resources become scarce. In this context, σ^{\max} is the maximal rate of starvation that occurs when the environment is devoid of resources. The full system describing resource and consumer dynamics is given by

$$\begin{aligned} \frac{d}{dt}C &= \lambda_C(R)C - (\mu + \sigma(R) + \dots)C, \\ \frac{d}{dt}R &= \alpha R \left(1 - \frac{R}{k} \right) - \left(\frac{\lambda_C(R)}{Y_C} + \rho \right) C, \end{aligned} \quad (3)$$

where the '...' denotes where additional mortality terms, described later, will be included. The dynamic outcomes of this system of equations include two trivial steady states at $(R^* = 0, C^* = 0)$ and $(R^* = k, C^* = 0)$, and one internal steady state where both the consumer and resource population coexist. Because the internal steady state cannot be concisely written, we do not report it here. See Table I for a description of parameters.

The rate laws describing resource consumption as well as consumer growth and mortality all vary as a function of consumer body mass M_C , where the consumer is assumed to be a mammalian herbivore, and the resource is an unspecified primary producer with characteristic growth rate, carrying capacity, and energy density E_d . We approach the derivation of vital rates with respect to consumer mass by solving for multiple timescales associated with ontogenetic growth, maintenance, and expenditure. The growth of an individual consumer from birth mass $m = m_0$ to its reproductive size $m = 0.95M_C$ is given by the solution to the general balance condition $B_0 m^\eta = E_m \dot{m} + B_m m$, where E_m is the energy needed to synthesize a unit of biomass, B_m is the metabolic rate to support an existing unit of biomass, and the metabolic exponent $\eta = 3/4$ [5]. From this balance condition, the time required for an organism starting from mass m_1 to reach mass m_2 follows

$$\tau(m_1, m_2) = \ln \left(\frac{1 - (m_1/M_C)^{1-\eta}}{1 - (m_2/M_C)^{1-\eta}} \right) \frac{M_C^{1-\eta}}{a(1-\eta)} \quad (4)$$

where $a = B_0/E_m$. From this general equation, we calculate the timescale of reproduction for an herbivore consumer of mass M_C as $t_\lambda = \tau(m_0, 0.95M_C)$, such that the reproductive rate is $\lambda_C^{\max} = \ln(\nu)/t_\lambda$, where $\nu = 2$ is the set number of offspring per reproductive cycle [9, 21]. The consumer yield coefficient is given by $Y_C = M_C E_d / B_\lambda$ (g consumer per g resource), where B_λ is the lifetime energy use required to reach maturity $B_\lambda = \int_0^{t_\lambda} B_0 m(t)^\eta dt$, and the maintenance rate is given by $\rho = B_0 M_C^\eta / M_C E_d$ [9].

To determine the rate of mortality from starvation, we calculate the time required for an organism to metabolize its endogenous energetic stores, estimated from its cumulative fat and muscle mass, where the remaining mass is given by $M_C^{\text{starve}} = M_C - (M_C^{\text{fat}} + M_C^{\text{musc}})$ (see Table I). During starvation, we assume that an organism burns its existing endogenous stores as its sole energy source, where the balance condition is altered to $\dot{m}E'_m = -B_m m$, where E'_m is the amount of energy stored in a unit of biomass (differing from the amount of energy used to synthesize a unit of biomass E_m). The starvation timescale is then given by

$$t_\sigma = -\frac{M_C^{1-\eta}}{a'} \ln(M_C^{\text{starve}}/M_C), \quad (5)$$

where $a' = B_0/E'_m$, such that the starvation rate is the $\sigma^{\max} = 1/t_\sigma$.

To determine the rate of mortality from aging, we note that population cohorts experience two primary sources

of natural mortality: the initial cohort mortality rate q_0 and the annual rate of increase in mortality as the cohort ages, or the actuarial aging rate, q_a over lifetime t_ℓ . We begin by assuming that the number of survivors over time follows a Gompertz relationship [9, 15] from which we can derive the average rate of natural mortality

$$\mu = \frac{q_0}{q_a t_\ell} (\exp(q_a t_\ell) - 1). \quad (6)$$

The three parameters (q_0, q_a, t_ℓ) each have well-documented allometric relationships for terrestrial mammals, such that natural mortality can be written as a function of consumer mass $\mu(M_C)$ (see Supplementary Materials Appendix 1).

We emphasize that while the sizes of physiological biomass compartments are obtained from empirical observations, the rates determining biomass flux are derived from process-based energetic relationships. Together, the allometric rate laws and the dynamic system presented in Eq. 3 allow us to assess the dynamics of consumer-resource systems for mammalian herbivores spanning the observed range of terrestrial body sizes, from the smallest (the Etruscan shrew at roughly 1 g) to the largest (the Oligocene paraceratheres and Miocene deinotheres at ca. $1.5 - 1.74 \times 10^7$ g) [22]. We next examine how this minimal framework is well-suited to provide general insight into several key allometric constraints that contribute to the functioning and limitations of terrestrial mammalian communities.

III. RESULTS AND DISCUSSION

A. Recovering Damuth's mass-density relationship

Our consumer-resource system is related to the nutritional state model (NSM) proposed in Yeakel et al. [9], where an explicit starvation dynamic was incorporated by separating the consumer population density into 'full' and 'hungry' states. Here we eliminate the transition between full and hungry states. Because the timescales of transitioning between full and hungry states are short relative to those of reproduction, we have only sacrificed a modest degree of physiological realism to enable analytical expression of steady states with additional sources of mortality. After substituting allometric relationships into the rate laws in Eq. 3, we observe that the internal steady state of the consumer is very close to observed mammalian densities, thereby approximating Damuth's Law (blue line in Fig. 1). Compared to the NSM [9], and similar to DeLong & Vasseur [23], we observe slightly exaggerated densities for small-bodied consumers, though within the observed range of variation. This overestimate is not observed when explicit starvation and recovery are included [9], suggesting these dynamics play an important role in depressing the populations of smaller-bodied species. Incorporating observed variations in measured values for α and k reveals strong alignment between

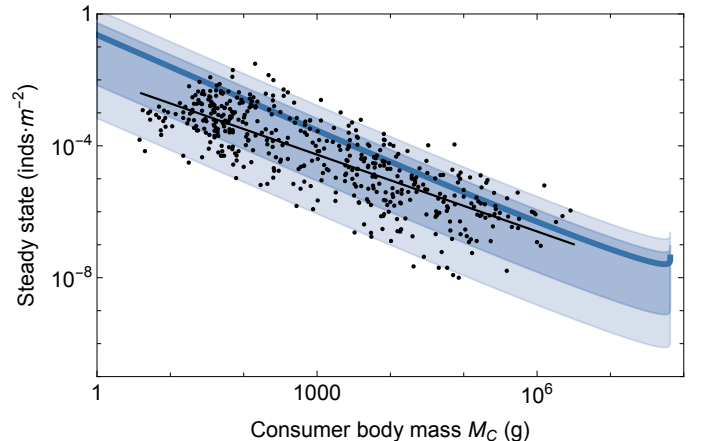


Figure 1: Model predictions of mammalian steady states ($\text{inds} \cdot \text{m}^{-2}$) as a function of herbivore consumer body mass M_C (thick blue line) compared to observational data from Damuth [19] (black points). Variation in steady state densities is captured by allowing the plant resource growth rate to vary as $\alpha = 2.81 \times 10^{-10} : 2.19 \times 10^{-8} \text{ s}^{-1}$ (dark blue shaded region), and both α and the plant resource carrying capacity to vary as $k = 2.3 : 34 \text{ kg/m}^2$ (light blue shaded region).

model predictions and the observed variability of densities across mammalian clades (Fig. 1). We examine the effects of variation for other vital rates in Supplementary Materials Appendix 2.

B. Natural mortality and starvation have an out-sized impact on smaller consumers

We first consider two internal sources of mortality: that due to the effects of aging, where mortality changes with an organism's temporal state, and that due to starvation, where mortality scales with an organism's energetic state. To understand the effect of changes to $\mu(M_C)$ on consumer steady states, we examine variations in the principle components of μ : initial cohort mortality q_0 and actuarial mortality q_a . The initial cohort mortality represents the mortality experienced by a cohort prior to accruing effects from age. We observe that the mortality rate changes proportionally with q_0 independent of consumer mass, where the ratio $\mu/\lambda_C^{\max} < 1$ even with respect to large increases in q_0 , unless q_a is similarly magnified (Fig. 2a,b). For survivorship mortality to approach the rate of reproduction ($\mu/\lambda_C^{\max} = 1$), where perceptible declines in population densities result, the initial cohort mortality must increase by roughly an order of magnitude (shaded region in Fig. 2c). Due to the steepness of the scaling of μ relative to λ_C^{\max} , this effect is felt exclusively by small-bodied organisms.

Actuarial mortality, q_a , represents the cumulative effects of aging, or senescence, across the organism's ex-

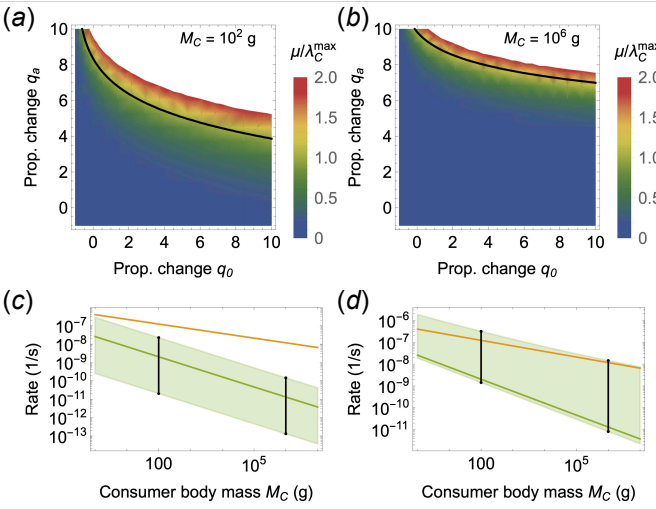


Figure 2: Changes in natural mortality as a function of initial cohort mortality q_0 , and actuarial aging, q_a for two different consumer body masses, M_c . The ratio reproduction λ_C^{\max} to natural mortality μ for a mammalian herbivore of (a) $M_C = 10^2$ g and (b) $M_C = 10^6$ g, across proportional changes to the initial cohort mortality rate q_0 and the actuarial aging rate q_a . The black contour denotes $\mu/\lambda = 1$. (c,d) Natural mortality μ (green) relative to reproduction λ_C^{\max} (orange) as a function of consumer body mass M_C . The range of variation (light green shaded region) shows proportional changes to the (c) cohort mortality rate q_0 and the (d) actuarial aging rate q_a from -0.99 to 10.

pected lifetime. We observe that as q_a increases, the magnitude of mortality increases disproportionately (Fig. 2a,b), while the slope of $\mu(M_C)$ becomes more shallow (Fig. 2d), primarily due to the cumulative nature of senescence magnifying its effects across the longer lifetimes of larger mammals. As such, an increase in q_a overwhelms reproduction such that $\mu/\lambda_C^{\max} > 1$, resulting in population instability (Fig. 2a,b). The extinction risk imposed by senescence has been explored across mammalian taxa, and while some life history characteristics such as the inter-birth interval appear to correlate strongly with these risks, the role of body size is notably ambiguous [16]. Though our model – which considers averaged effects across terrestrial mammals – predicts that the risks of increased actuarial mortality are disproportionately felt by smaller size-classes, we also show that μ increasingly resembles λ_C^{\max} with increasing q_a (the top border of the shaded region in Fig. 2d). This increased similarity implies that relatively small variations in other demographic processes or interactions may have potentially large and destabilizing effects on population size that cannot be predicted from body mass, a potential source for the noted ambiguity between size and actuarial extinction risk [16].

While the temporal state of an organism is unidirec-

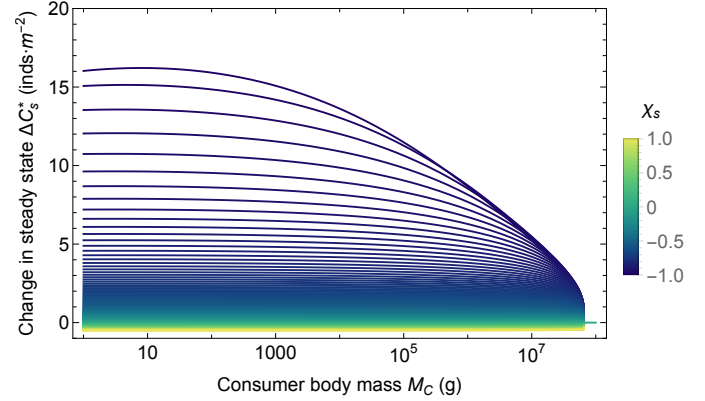


Figure 3: The relative change in consumer steady state ΔC_s^* as a function of consumer body mass M_C given an altered rate of starvation $\sigma(R) \cdot (1 + \chi_s)$ across the proportional change $\chi_s \in (-0.99, 1)$.

tional and linear, other internal states, such as an organism's energetic state, fluctuate nonlinearly over time. In this case, the rate of starvation is low when resources become plentiful ($R \rightarrow k$) and increases to σ^{\max} as resources become scarce ($R \rightarrow 0$). Because organisms metabolize their fat and muscle tissue during starvation, and die from starvation when these energetic stores are metabolized, the timescale of starvation varies with the amount of endogenous energetic stores an organism carries. Larger organisms carry a larger proportion of body mass as fat [4], such that they are more protected from the effects of short-term resource scarcity [24]. We observe this effect by modifying the starvation rate and examining how the steady state population size is altered. We introduce variation to the rate of starvation as $\sigma(R) \cdot (1 + \chi_s)$, from which the altered steady state C_s^* is calculated. The relative change in steady states introduced by the altered starvation rate is then given by $\Delta C_s^* = (C_s^* - C^*)/C^*$, where positive values indicate a relative gain in steady state densities from the proportional change χ_s , and negative values indicate a relative loss (Fig. 3). We observe that, while all mammals benefit from reduced starvation rates ($\chi_s < 0$), smaller-bodied mammals benefit to a much greater extent, and this effect tapers off with increasing body mass. Because fat biomass scales super-linearly with body mass, the populations of larger consumers are more resilient to the effects of starvation, whereas those of smaller consumers are more prone.

An organism's rate of starvation emerges from two governing forces – the amount of energy storage and the rate of its use – and as such can be manipulated both physiologically and behaviorally. For instance, behaviorally supplementing endogenous fat stores with exogenous caches magnifies an individual's energetic stores [25], whereas physiologically-mediated responses to starvation risk such as torpor can introduce significant temporal delays to the effects of resource scarcity [26]. In

both cases the time required to pass from a replenished to a starved state is effectively increased, lowering the rate of starvation. The predicted benefits of such adaptations to mammalian steady state densities will be realized primarily by smaller mammals (Fig. 3, Supplementary Materials Appendix 2), and it is these size classes where traits such as caching and torpor are most commonly observed [25, 27, 28].

C. Predation mortality and the feasibility of megatrophic interactions

Predators introduce an external source of mortality on prey populations, fueling their own population growth in whole (trophic specialists) or in part (trophic generalists), by the rate at which prey are consumed. We account for the effects of an implicit predator density P with body size M_P on the herbivore consumer density C with body size M_C . The mortality rate of the herbivore consumer from an external predator is given by

$$\beta(C, P) = w \frac{\lambda_P(C)P}{CY_P}, \quad (7)$$

where $\lambda_P(C)$ is the growth rate of the predator and Y_P is the predator yield coefficient, describing the grams of predator produced per gram of prey consumed (see Supplementary Materials Appendix 3), and w is the predator's specialization ($w = 1$ denotes specialization, whereas $w < 1$ denotes generalization). Assuming a linear functional response for predation mortality, $\lambda_P(C)$ is maximized when the consumer reaches its theoretical maximum population density, which we calculate by converting the resource carrying capacity directly to grams of consumer produced, or $C^{\max} = Y_C k$. While this is an ultimately unattainable theoretical bound, it allows for a direct calculation of the predator growth rate as a function of C , written as

$$\lambda_P(C) = \lambda_P^{\max} \frac{C}{C^{\max}} = \lambda_P^{\max} \frac{C}{Y_C k}, \quad (8)$$

where λ_P^{\max} is the maximum predator growth rate. The theoretical boundary density for herbivore consumers C^{\max} can similarly be used to calculate the boundary density for predators, $P^{\max} = Y_P C^{\max}$, both of which accurately capture the upper-bounds of herbivore and carnivore mass-density observations (dashed lines in Fig. 4a). Because the effects of the predator are implicit, we assume that the predator population remains at empirically measured steady state densities for mammalian carnivores, where $P \equiv P^* = P_0 M_P^{-0.88}$ (Table I) [29].

The predation mortality rate depends on both the body size of the herbivore consumer and its respective predator. Trophic interactions are constrained by body size [30–32], and large prey generally suffer mortality from large predators, though the nature of predator-prey mass ratios (PPMRs) varies across communities [33],

body size [31, 34–37], and is not well understood outside of aquatic gape-limited systems [38]. Because our framework is prey-centric, we require a prediction of the expected predator mass given an herbivore of body size M_C . For larger predators and prey ($> 10^5$ g) [39–44], the expected predator mass given a particular herbivore mass follows roughly $E\{M_P\} = v_0 M_C^{v_1}$, where $v_0 = 9.76 \times 10^3$ g and $v_1 = 0.21$ (Fig. 4b; see Supplementary Materials Appendix 3). Accordingly, larger terrestrial herbivores tend to suffer mortality from proportionately smaller predators, an asymmetry that becomes more pronounced with increasing size [cf. 30]. We note that smaller terrestrial predator/prey size classes tend to follow different PPMR relationships, where predators tend to be much larger than prey (e.g. rodent- or insect-specialist mesocarnivores) [45, 46]. Here and throughout the prefix 'mega' is used to signify size classes $> 5 \times 10^5$ g [39].

Integrating the large-bodied PPMR relationship into the predation mortality rate reveals the emergence of a dynamic instability at megaherbivore size classes (Fig. 4a,b). An implicit predator population with body size $E\{M_P\}$ is thus able to withdraw sufficient biomass from an herbivore prey population to sustain itself, without crashing the herbivore population, below a threshold herbivore size of $M_C^\dagger = 2.58 \times 10^6$ g (Fig. 4a). Above this critical size threshold, the herbivore population has such low densities that it is unable to sustain a specialist predator species large enough to consume it, introducing a strong upper-bound to mammalian carnivore body size driven by a trophic cascade. This boundary matches the herbivore maximum size limit observed in contemporary terrestrial systems, at roughly the size of an elephant [30] (Fig. 4b; Supplementary Materials Appendix 3).

While M_C^\dagger marks the threshold herbivore mass above which predation is unsustainable, Sinclair et al. [30] have shown contemporary herbivores to begin to escape predation at ca. 4.22×10^5 g. This change-point reflects the limitations of contemporary carnivores, which reach a maximum body size of 1.15 to 2.60×10^5 g [30], and have preferences for prey up to 5.50×10^5 g [39]. As such, the sole predators of contemporary giants are not megaherbivore specialists, instead opportunistically subsidizing their preferred prey base. While we have so far assumed a specialized predator-prey interaction, the largest predators in natural systems tend to be dietary generalists [30, 47]. We observe that increasing the implicit dietary generality of the predator (such that $w < 1$) increases M_C^\dagger to a larger threshold mass (Fig. S3). For example, $w = 0.37$ means that a predator is supporting a little more than 1/3 of its growth rate by the targeted prey, increasing the herbivore body mass boundary to $M_C^\dagger = 1.75 \times 10^7$ grams (Fig. 4b; Supplementary Materials Appendix 3), roughly the body mass attained by the largest terrestrial herbivores, the Oligocene paraceratheres and Miocene deinotheres [9, 22].

That the threshold herbivore mass decreases with increasing predator specialization suggests that larger predators are dynamically constrained to be dietary gen-

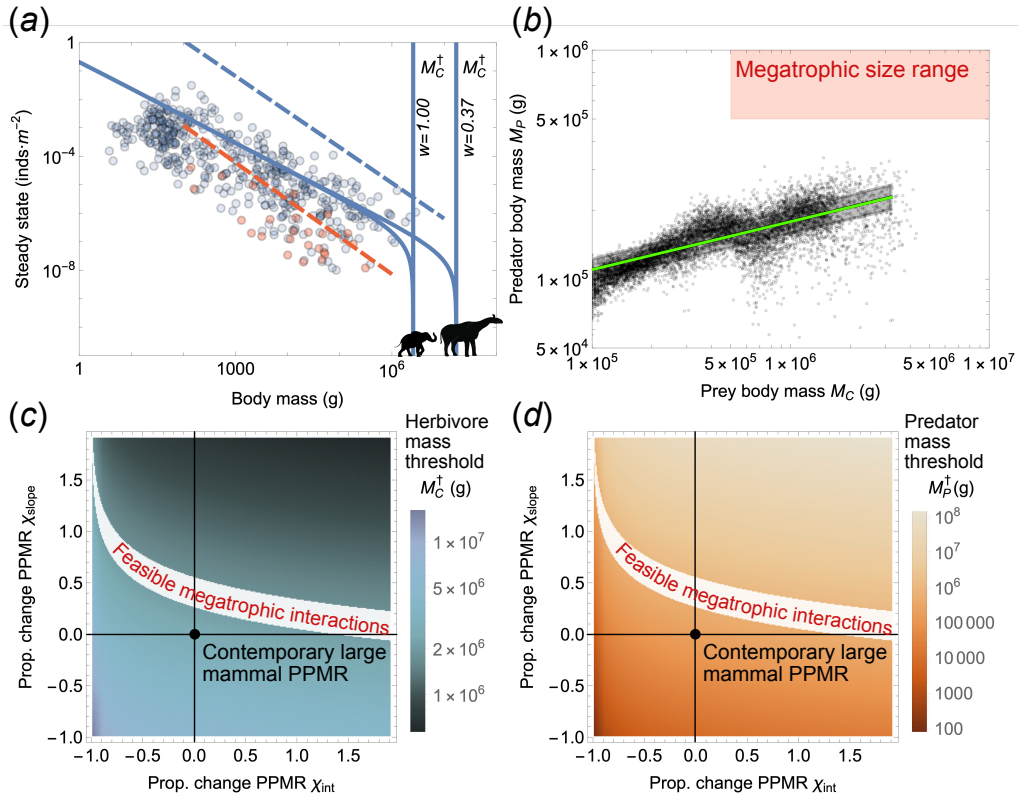


Figure 4: The feasibility of predation. (a) Empirical mammalian herbivore (blue points) and predator (red points) mass-densities shown alongside the theoretical maximum herbivore C^{\max} and predator P^{\max} densities across body size (dashed lines). The solid blue curves denote the predicted herbivore consumer steady state $C^*(M_C)$ with predation mortality given specialist ($w = 1$) and generalist ($w = 0.37$) predation. (b) Predator body mass as a function of prey body mass observed among contemporary mammalian fauna provides the allometric predator-prey mass ratio (PPMR). Data bootstrapped from empirical observations in Refs. 39–44. The green line denotes the best fit, where $M_P = 9.76 \times 10^3 M_C^{0.21}$. The red shaded region denotes megafaunal size ranges, which are not captured by contemporary predator-prey interactions. (c) Threshold herbivore sizes M_C^\dagger and (d) carnivore sizes M_P^\dagger across changes to the PPMR intercept χ_{int} and slope χ_{slope} (see Eq. S22). White shaded region denotes megatrophic threshold sizes, where both $(M_C^\dagger, M_P^\dagger) > 6 \times 10^5$ g.

eralists [30], while also pointing to an amplifying feedback mechanism [12] that may operate in diverse communities undergoing megafaunal extinctions. As megaherbivore species are lost, the largest predators must respond by increasing their reliance on those remaining. Our results reveal that this energetic redirection will reduce the threshold herbivore mass M_C^\dagger to lower size classes, thereby promoting additional extinctions and attendant predator specialization, a quantitative assessment of the previously proposed influence of top-down dietary ratcheting [48, 49].

While deinotheres and paraceratheres top the megaherbivore scale, the Eocene artiodactyl *Andrewsarchus* may have been the largest terrestrial mammalian predator at up to 1×10^6 g [50], while the Miocene Hyenaodontid *Megistotherium osteothlastes* ranged between 5 to 8×10^5 g and the early Eocene Oxyaenodont *Sarkastodon mongoliensis* weighed ca. 8×10^5 g [51]. A theoretical

maximum mammalian carnivore size of 1.1×10^6 g has been proposed based on the intersection of daily energetic uptake requirements against metabolic expenditures [52], closely aligning with the largest known megapredators. While our consumer-resource framework provides a range of predicted megaherbivore body mass thresholds depending on the fraction of predator growth it fuels, we next ask under what conditions megatrophic relationships between megaherbivores and megapredators are dynamically feasible.

A principle relationship in our framework is the allometric PPMR observed for the largest contemporary herbivores and carnivores, however this PPMR cannot account for past megatrophic relationships (Fig. 4b; Supplementary Materials Appendix 3). While it is unknown whether these super-sized carnivores were specialists on deinotheriid size-classes, our framework allows us to investigate whether and to what extent changes to the con-

temporary PPMR enable megatrophic interactions (Fig. 4c-d), where we allow the expected predator mass given a particular prey mass to vary as

$$E\{M_P\} = v_0(1 + \chi_{\text{int}})M_C^{v_1(1 + \chi_{\text{slope}})}, \quad (9)$$

and where the proportional changes in the PPMR intercept and slope are given by χ_{int} and $\chi_{\text{slope}} \in (-0.99, 2)$. We observe that only a small range of values for PPMR intercepts and slopes permit the existence of dynamically feasible megatrophic interactions, where megaherbivores serve as prey for megapredators (white band in Fig. 4c,d; Fig. S4). While significantly larger PPMR intercepts ($\chi_{\text{int}} \gg 0$) are unlikely to be realized in natural systems, the megainteraction range does include very low intercepts with very high slopes, such that PPMRs are low at smaller masses, and much higher at large masses.

Feasible megatrophic interactions increase substantially if a smaller percentage of the predator growth rate is fueled by the target herbivore population ($w < 1$). Setting $w = 0.37$ – which we observed increases M_C^\dagger to deinothere/indricothere size classes – and allowing both χ_{int} and χ_{slope} to vary, results in megatrophic interactions spanning the largest megaherbivore and megapredator sizes observed in the fossil record (Supplementary Materials Appendix 3; Fig. S5). That increased generality favors megatrophic feasibility agrees with previous conjectures that the largest mammalian terrestrial predators were likely dietary generalists [53]. Our framework highlights dynamic constraints existing between predators and prey that may serve to structure mammalian communities over evolutionary time, in particular revealing the tenuous positions of mega-sized herbivores and predators. As carnivorous clades acquire body sizes enabling megaherbivore predation over evolutionary time, their super-sized appetites may have resulted in unsustainable megaherbivore densities where the risk of extinction is overwhelming – an evolutionary trap marking the final tooth in the hypercarnivore ratchet [cf. 54].

D. Harvesting to extinction

We last consider the effects of anthropogenic harvest-induced mortality on herbivore populations. While the predation rate is naturally limited by the energetic needs of the predator, we consider harvest to be a comparatively unconstrained source of mortality. This may be the case if the human population(s) engaged in harvesting are subsidized by alternative resources [55]. Harvest pressure has potentially varying relationships with consumer (prey) body mass, a complex product of environment, climate, culture, and technology [56]. For example, hunting traditions specializing on mass-collecting, by way of trapping or netting [56, 57] are expected to exhibit harvest allometries biased towards smaller species, whereas a purely opportunistic strategy may be expected

to have very little allometric dependence. While smaller mammals do not appear to offer a significant return on investment, the mass-collecting of invertebrates such as grasshoppers, and fish can offer significant returns [57]. In contrast, the innovation of advanced projectiles is thought to have enabled harvest of terrestrial megafauna [56, 58], while archeological evidence points to many Pleistocene human populations as potential megafaunal specialists [59].

Because harvest scaling may be difficult to measure and idiosyncratic, we calculate the harvest rate required to induce extinction, h^\dagger , as a function of body size M_C , and find a scaling relationship proportional to the mass-density relationship where $h^\dagger \propto M_C^{-1/4}$. This is a natural result, as the effort required to suppress a population is expected to be proportional to the consumer's abundance, reflecting the increased susceptibility of large-bodied organisms to extinction [60]. As a proportion of the other sources of consumer mortality that we have considered (excluding predation; $w = 0$), extinction-level harvesting is lower for smaller consumers, saturating at close to unity for larger consumers, reflecting the elevated role of starvation mortality among smaller-sized organisms (Fig 5A). With predation mortality included from both generalist ($w = 0.37$) and specialist ($w = 1$) predators, extinction-level harvesting accounts for an increasingly smaller proportion of mortality for larger organisms (orange and red lines, Fig. 5a). This highlights the delicate nature of the megafaunal niche, where smaller changes in mortality rates can induce population collapse [60].

To examine how our estimate of extinction-level harvesting rates h^\dagger compare to those estimated for human hunting of paleontological and historical mammalian populations, we converted h^\dagger to harvest pressure ψ^\dagger , or the number of individuals harvested per year to reduce the population to a fraction of its steady state ϵC^* where we set $\epsilon = 0.01$. We calculate ψ^\dagger for an arbitrary area (see Supplementary Materials Appendix 4), which we standardize as the area of California ($A_{\text{CA}} = 4.24 \times 10^5 \text{ km}^2$), such that

$$\psi^\dagger \propto -h^\dagger \frac{C^*(1 - \epsilon)}{M_C \log(\epsilon)}. \quad (10)$$

Though the annual harvesting pressure is unrealistically high for smaller organisms, we observe that it is ca. $4.3 \times 10^3 \text{ inds/yr}/A_{\text{CA}}$ for elephant-sized organisms (ca. $2.5 \times 10^6 \text{ g}$) in the absence of predation mortality ($w = 0$). With the increasing pressures of generalist and specialist predation, the harvest pressure required to induce extinction is much less for these larger consumers (orange and red lines in Fig. 5b). We note that this calculation of harvest pressure should be viewed as a minimum estimate given that we do not account for demographic rebound. As such, this measure is appropriate only if the timescale of harvest is less than the generational timescale, which is the case for the megafauna considered here.

Our predictions of extinction-inducing harvest pres-

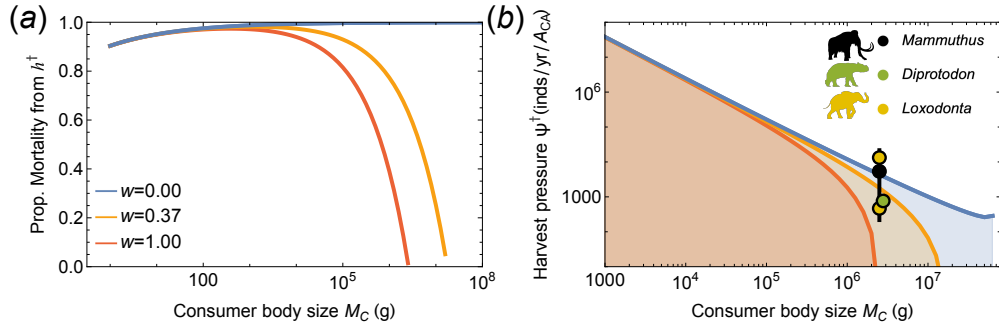


Figure 5: The effects of harvest mortality on herbivore consumers. (a) Proportion mortality due to an extinction-inducing harvest rate ξ^\dagger without predation ($w = 0$; blue line), and with mortality from a generalist predator ($w = 0.37$; orange line) or a specialist predator ($w = 1$; red line), as a function of consumer body mass M_C . (b) Harvest pressure ψ^\dagger (inds/yr/ A_{CA}) without predation ($w = 0$; blue line), with the inclusion of mortality from a generalist predator ($w = 0.37$; orange line), and with the inclusion of mortality from a specialist predator ($w = 1$; red line), as a function of consumer body mass M_C . Black point and line: median and range of estimated harvest rates for wooly mammoths (*Mammuthus primigenius*) [61]; Green point: estimated harvest pressure for the Australian *Diprotodon* [13]; Lower and upper yellow point: estimated harvest rates for contemporary *Loxodonta* during the early 1800s and just prior to 1987, respectively [62].

sure compare well with paleontological and historical estimates of harvest pressure on mammalian megafauna (see Supplementary Materials Appendix 4 for details). For example, Fordham et al.’s [61] estimate of the harvest pressure required to collapse mammoth (*Mammuthus primigenius*) populations (using a formulation similar to that of Alroy; [11]) reveals a range of values consistent with our expectation for similar size-classes (est. harvest pressure = 1.24×10^4 inds/yr/ A_{CA}), as did estimates of extinction-inducing harvest of the Australian *Diprotodon* (est. harvest pressure = ca. 763 inds/yr/ A_{CA} ; [13]). Within the historical record, elephant (*Loxodonta*) populations experienced comparatively lower harvest pressure through 1850 (ca. 466 inds/yr/ A_{CA} , derived from the volume of ivory exports; [62]). While fluctuating over the next century, harvest pressure elevated to a maximum of ca. 13.3×10^5 inds/yr/ A_{CA} just prior to 1987 (Fig. 5b). This level of harvest was not sustained, as ivory export volume plummeted following the implementation of trade restrictions in 1989 [62]. Both Fordham et al.’s [61] estimate for Pleistocene mammoths and the short-lived harvest maximum for African elephants in 1987 [62] achieved pressures greater than ψ^\dagger under the conservative assumption of no natural predation. While estimates for *Diprotodon* harvest are considerably lower [13], it is important to note that our framework is parameterized for eutherian rather than marsupial mammals. Nevertheless, the estimated *Diprotodon* ψ^\dagger is well within range of extinction-inducing harvest rates if natural predation pressures are also included, and there is evidence to suggest that *Diprotodon* likely served as prey for marsupial lions [63, 64], and both giant crocodylians (*Pallimnichthys*) and varanid lizards (*Megalania*) [65].

IV. CONCLUSION

We have shown that the inclusion of mass-specific energetic transfer between resources and consumers, combined with the unique timescales governing consumer mortality, both predict Damuth’s Law [19] and provide insight into dynamic thresholds constraining populations. While natural and starvation mortality primarily impact small-bodied species, trophic mortality primarily impacts large-bodied species with longer generational timescales. Moreover, while mass-specific predation gives rise to dynamic thresholds on herbivore populations, these effects are sensitive to both predator generality as well as the associated predator-prey mass ratio, which isn’t well understood in terrestrial ecosystems [38]. While assessment of particular communities and/or species requires more detailed approaches – integrating, for example, life history dynamics as in Bradshaw et al. [13] – we suggest that a general and lower-dimensional framework may be useful for extracting first-order energetic constraints that both shape and potentially limit the nature of mammalian communities.

That extinction risk appears to increase with body size [66] is integral to our understanding of the Pleistocene extinctions [11–13, 59, 67] and anthropogenic effects throughout the Holocene [68]. Because megafaunal loss may have disproportionately large impacts on ecosystem functioning [60], understanding the mechanistic drivers that may lead these species to the brink is of paramount importance. Assessing which energetic walls close in and why as body size increases, is a fundamental aspect of reconciling the nature of extinction [12], particularly when there is size-selectivity [59]. That we observe dynamically-feasible megatrophic interactions to occupy a narrow band of PPMR relationships points

to a broader range of interaction structures than are realized in contemporary communities. As the threshold consumer mass decreases with predator specialization, how megafaunal trophic structure changes during extinction cascades may be central for understanding the dynamics of community disassembly [36]. And while these dynamics may arise naturally from the energetic limitations of mammalian interactions, it may be that the added pressure of subsidized harvest, particularly on megafauna, inevitably leads to collapse.

Code available on GitHub: https://github.com/jdyeakel/2022_mortality

TR and JDY conceived of the study. TR, CK, and JDY designed the model and analyzed the results. TR, CK, and JDY wrote the manuscript.

We would like to thank Irina Birskis-Barros, Uttam Bhat, Jessica Blois, Nathaniel Fox, Jacquelyn Gill, Emily Lindsey, Megha Suswaram, and Ritwika VPS for insightful comments and discussions that greatly improved the ideas and concepts that contributed to this manuscript.

Table I: Model parameters and values/units

Definition	Parameter	Value/Units
Resource		
density	R	g/m ²
reproduction rate	α	1/s
carrying capacity	k	g/m ²
Consumer		
density	C	g/m ²
body mass	M_C	g
body mass threshold	M_C^\dagger	g
theoretical max	C^{\max}	g/m ²
timescale of growth from m_1 to m_2	$\tau(m_1, m_2)$	s
reproduction rate	λ_C^{\max}	1/s
yield coefficient	Y_C	(g/m ² C)/(g/m ² R)
maintenance rate	ρ	1/s
natural mortality rate	μ	1/s
starvation rate	σ^{\max}	1/s
harvest rate	h	1/s
Predator		
steady state intercept	P_0	8.62×10^{-4} inds/m ² [29]
steady state density	P^*	$P_0 M_P^{-0.88}$ inds/m ² [29]
body mass	M_P	g
body mass threshold	M_P^\dagger	g
theoretical max	P^{\max}	g/m ²
growth rate	λ_P^{\max}	1/s
yield coefficient	Y_P	(g/m ² P)/(g/m ² C)
specialization	w	(0,1)
Prop. change starvation rate	χ_s	(-0.99,1)
PPMR intercept	v_0	1.18×10^5 g
PPMR slope	v_1	0.19
Prop. change PPMR intercept	χ_{int}	(-0.99,2)
Prop. change PPMR slope	χ_{slope}	(-0.99,2)
Extinction-inducing harvest rate	h^\dagger	1/s
Extinction-inducing harvest pressure	ψ^\dagger	inds/yr/ A_{CA}
Post-harvest fraction consumer density	ϵ	0.01

V. SUPPLEMENTARY APPENDICES

SUPPLEMENTARY APPENDIX I. NATURAL MORTALITY

The natural mortality rate is obtained by first assuming that the number of surviving individuals in a cohort N follows a Gompertz relationship [15], where

$$N = N_0 \exp \left(\frac{q_0}{q_a} \left(1 - \exp(-q_a t) \right) \right), \quad (\text{S11})$$

given that q_0 is the initial cohort mortality rate, and q_a is the annual rate of increase in mortality, or the actuarial mortality rate. The change in the cohort's population over time then follows

$$\frac{d}{dt} N = -dN, \quad (\text{S12})$$

such that

$$d = -\frac{1}{N} \frac{d}{dt} N. \quad (\text{S13})$$

If t_ℓ is the expected lifetime of the organism, then the average rate of mortality over a lifetime t_ℓ is

$$\begin{aligned} \mu &= \frac{1}{t_\ell} \int_0^{t_\ell} q_0 \exp(q_a t) dt \\ &= \frac{q_0}{q_a t_\ell} \left(\exp(q_a t_\ell) - 1 \right). \end{aligned} \quad (\text{S14})$$

The cohort mortality rate q_0 , the actuarial mortality rate q_a and the expected lifetime t_ℓ of a mammal with mass M_C all follow allometric relationships, where $q_0 = 1.88 \times 10^{-8} M_C^{-0.56}$ (1/s) and $q_a = 1.45 \times 10^{-7} M_C^{-0.27}$ (1/s) where M_C is in grams. Together, we obtain the allometric relationship

$$\mu(M_C) = \frac{3.21 \times 10^{-8} (\exp(0.586 M_C^{0.03}) - 1)}{M_C^{0.59}}. \quad (\text{S15})$$

SUPPLEMENTARY APPENDIX II. VARIATIONS IN MODEL PARAMETERS AND ALLOMETRIC RATES

While our framework dictates that plant growth rates and carrying capacities are directly proportional to consumer steady states, we can gain insight into what drives the very large range of observed consumer densities by exploring the observed ranges of α and k in terrestrial systems. We assume an intrinsic growth rate roughly that of grass where $\alpha = 9.45 \times 10^{-9}$ (s⁻¹), whereas observations among terrestrial plants reveal a range in growth rates from 2.81×10^{-10} to 2.19×10^{-8} [69], according with a change in α of roughly 97% lower and 130% higher than the set value. By incorporating this range into the estimated resource growth rate, we observe that

we can account for a large portion of consumer steady state densities around the mean density (inner shaded region, Fig. 1, main text). If we additionally adjust the carrying capacity k of the resource to 90% less-than and 150% more-than the assumed value of 23×10^3 g/m², our framework accounts for nearly the full range of mammalian steady state densities (outer shaded region, Fig. 1, main text). In this context, the upper-boundary of k observed to capture most higher herbivore densities is ca. 34 kg/m², which is on the higher end of estimated live above-ground biomass densities in terrestrial forests such as in Isle Royal and the Allegheny National Forest [70].

Our model's ability to capture the bounds of mammalian densities at low and high productivity invites some speculation into the actual steepness of the mass-density relationship. While the best-fit slope to Damuth's Law is -0.77 we also observe that the steeper relationship given by our framework better captures the boundaries of mass-density data, whereas varying the intercept of the statistical best-fit would not capture the lower-density outer-boundary of larger species. While within-clade mass-density relationships often reveal a shallower slope than if measured across clades [71], it is possible that the absence of data for larger mammals may bias estimates of the slope towards smaller (shallow) values. Mammalian communities have undergone significant anthropogenic restructuring throughout the Holocene (REF), such that many larger species are excluded from the mass-density relationship by way of extinction [72], and the greater prevalence of smaller species may introduce size-dependent biases. For example, if species < 100 g are excluded, the empirical mass-density slope steepens from -0.77 to -0.85.

Considering how variations to the underlying energetic parameters driving consumer-resource dynamics alters the expected mass-density relationship may shed light on key constraints shaping mammalian communities. We next explore how variations in the vital rates included in the consumer-resource model modify the expected intercept and slope of the mammalian mass-density relationship. Different vital rates impact the mass-density relationship in three distinct ways, by either *i*) influencing only the mass-density slope, *ii*) influencing only the mass-density intercept, or *iii*) influencing both. Aside from the resource growth rate and carrying capacity, our framework also includes the intrinsic consumer reproductive rate λ_C^{\max} , the consumer yield coefficient Y_C , and the maximum rate of starvation σ^{\max} . We introduce changes to these rates as, for example, $\lambda_C^{\max'} = \lambda_C^{\max}(1+\chi)$, where $\chi \in (-1, 2)$ represents the proportion increase or decrease of the altered parameter denoted by $'$. We note that the recovery rate ρ is sufficiently small that alterations do not have an influence on either the consumer mass-density intercept or slope.

Importantly, changes to the starvation rate have a large effect on both the consumer-density intercept and slope (Figs. S1,S2). We observe that decreasing σ^{\max} from the expected value ($\chi < 0$) serves to increase the

steady state intercept, while decreasing the mass-density slope. By comparison, increasing σ from the expected value ($\chi > 0$) has less effect on the mass-density relationship. In the consumer-resource model described in Eq. 2.3 (main text), starvation is the primary source of consumer mortality, and therefore plays an out-sized role in determining consumer steady states. As this mortality is reduced, consumer densities increase, raising the intercept. However, as consumer starvation rates decline we observe a steeper mass-density slope. Reduced starvation rates therefore principally benefit the steady state densities of smaller species, with reduced effects observed for larger-bodied mammals. Because fat biomass scales super-linearly with body mass (see Table 1, main text), the populations of larger consumers are more resilient to the effects of starvation, whereas those of smaller consumers are more prone.

The consumer's maximal rate of reproduction λ_C^{\max} influences only the mass-density slope except for the case $\chi \rightarrow -1$, where growth becomes zero. Above this trivial limit, we observe the consumer growth rate to have a negative effect on the mass-density slope, such that as the growth rate increases, the mass-density relationship becomes steeper (Figs. S1,S2). As the intercept does not change, this means that the steady states of larger bodied consumers decline with increasing λ_C^{\max} , while those of smaller-bodied consumers remain unaltered, though the effect is slight. Of more interest is the effect of the yield coefficient Y_C and starvation rate σ^{\max} (Figs. S1,S2). The yield coefficient represents the conversion of resources to consumer biomass, where an increase in χ correlates to large increases in consumer steady state without altering the mass-density slope. Here we observe that increased efficiency in converting resource to consumer biomass will have an effect similar to increasing resource productivity, as the effective abundance of the resource is greater when relatively fewer resources fuel a given unit of consumer biomass. Because $Y_C \propto E_d$, where E_d is the energy density of the resource (see methods), resource quality is therefore expected to translate directly to higher consumer steady state densities.

SUPPLEMENTARY APPENDIX III. MORTALITY FROM PREDATION

Per-capita mortality rate from predation The per-capita mortality rate from predation of the herbivore consumer with mass M_C and population density C by a mammalian predator with body mass M_P and population density P is given by

$$\beta(C, P) = w \frac{\lambda_P(C)P}{CY_P}, \quad (\text{S16})$$

where $\lambda_P(C)$ is the growth rate of the predator, Y_P is the predator yield coefficient, describing the grams of predator produced per gram of prey consumed, and w is the degree of specialization of the predator on the consumer

prey ($w = 1$ denotes specialization, whereas $w < 1$ denotes generalization). Assuming a linear functional response for predation mortality, $\lambda_P(C)$ is maximized to λ_P^{\max} when the consumer reaches its theoretical maximum population density, which we calculate by converting the resource carrying capacity directly to grams of consumer produced, or $C^{\max} = Y_C k$. The growth rate of the predator is then given by

$$\lambda_P(C) = \lambda_P^{\max} \frac{C}{C^{\max}} = \lambda_P^{\max} \frac{C}{Y_C k}. \quad (\text{S17})$$

Together, we observe the per-capita mortality rate to be (as expected) independent of the consumer density C , and is simplified to

$$\beta(P) = w \frac{\lambda_P^{\max} P}{Y_P Y_C k}, \quad (\text{S18})$$

where we assume that the predator population remains at empirically measured steady state densities for mammalian carnivores, where $P \equiv P^* = P_0 M_P^{-0.88}$ [29]. This assumption is required because the effects of predation are implicit rather than explicit, and effectively assumes that predator populations operating far below this relationship are not viable. While there is bound to be a range of viable densities for a predator of a given body size, that mass-density relationships exist at all indicates that population densities are highly constrained and therefore represent a predator energetic demand as a function of body size. Accordingly, if the predator mass-density relationship P^* represents an expected energetic requirement for a functioning predator population, our assumption of predation as a constant, rather than dynamic, influence on herbivore mortality reveals the dynamic consequence of such energetic relationships. We suggest that it is these energetic mismatches that may constrain longer-timescale macroevolutionary forces, even if the shorter-timescale ecological dynamics may be more idiosyncratic and complex than our minimal model captures.

Herbivore and predator yields As described in the main text, consumer yield is calculated

$$Y_C = \frac{M_C E_d}{\int_0^{t_{\lambda_C}} B_0 m(t)^\eta dt}, \quad (\text{S19})$$

where E_d is the energy density of the plant resource R (Joules/g) and the denominator is the lifetime energy use required by the herbivore consumer to reach maturity (Joules). The parameters t_{λ_C} and B_0 are the timescale associated with reaching reproductive maturity and the metabolic coefficient for herbivorous mammals, respectively, and $\eta = -3/4$ is the metabolic exponent (see Table 1, main text). The predator yield is calculated similarly, where

$$Y_P = \frac{M_C E_C}{\int_0^{t_{\lambda_P}} B_0 P m(t)^\eta dt}, \quad (\text{S20})$$

where E_C is the energy density of the herbivore being consumed, and the denominator is the lifetime energy use required by the predator to reach maturity. The parameters t_{λ_P} and B_{0P} are the timescale associated with reaching reproductive maturity and the metabolic coefficient for predatory mammals, respectively, and $\eta = -3/4$ is the metabolic exponent. We note that the metabolic coefficient for predators is different than that for mammals [73].

The energy density of herbivore consumers changes with body mass M_C . For example, small mammals have very low percent body fat, whereas very large mammals have high percent body fat. We assume that predators consume all non-skeletal mass of prey. Because the amount of consumable tissues with different energy densities within an herbivore varies allometrically, so too should the energy density E_C . We consider four primary tissue groups: a consumable set composed of muscle, fat, and *other* tissues, and an non-consumable set composed only of skeletal tissues. If the scalings associated with fat, muscle, and skeletal tissues are $M_C^{\text{fat}} = f_0 M_C^{1.19}$, $M_C^{\text{musc}} = g_0 M_C^{1.00}$, and $M_C^{\text{skel}} = h_0 M_C^{1.09}$, the scaling of the *other* tissue (gut tissue, organ tissue, etc) is given by $M_C^{\text{other}} = M_C - (M_C^{\text{fat}} + M_C^{\text{musc}} + M_C^{\text{skel}})$ [74]. The energy density of fat is $E_{\text{fat}} = 37700 \text{ J/g}$, whereas the energy density of muscle is $E_{\text{musc}} = 17900 \text{ J/g}$ [75]. If we assume that gut and organ tissues have roughly the same energy density as muscle, the attainable energy density for an herbivore of size M_C is given by

$$E_C(M_C) = E_{\text{fat}} \frac{M_C^{\text{fat}}}{M_C} + E_{\text{musc}} \left(\frac{M_C^{\text{musc}}}{M_C} + \frac{M_C^{\text{other}}}{M_C} \right). \quad (\text{S21})$$

Large-bodied Predator-Prey Mass Ratio (PPMR) The predator growth rate λ_P^{\max} , the time required for the predator to reach reproductive maturity t_{λ_P} , and the predator's steady state population density P^* are allometric relationships that depend on its body mass M_P . Accordingly, for an herbivore of a given mass M_C , we must anticipate the size of its likely predator M_P . This is very different than the more typical issue of anticipating the average prey size for a given predator. For example, the most preferred prey mass for an African lion is ca. 350 kg [39], where the inclusion of megaherbivores to diet is comparatively low. However from a megaherbivore's perspective, lions may represent the only potential predator. In other words, because the range of prey body mass increases for predators of larger body mass [30], it is the upper limit of the range that impacts the populations of larger herbivores.

To obtain an herbivore-centric measure of the expected predator mass given a particular herbivore mass $E\{M_P|M_C\}$, we first compiled the known diets of large-bodied predators, including tigers, lions, hyenas, leopards, dhole, wild dogs, and cheetahs [39–44]. Because smaller mammalian predators and prey have very differ-

ent PPMR relationships than larger-bodied mammalian predators and prey, we here focus exclusively on the predators of large-bodied herbivore prey $> 10^5 \text{ g}$. From the mean proportional reliance of predators on large-bodied prey [39–44], we repeatedly sampled predator dietary distributions to reflect each predator's reliance as a function of prey mass. We introduced variability in predator and prey masses by assuming that body sizes were normally distributed about the expected value with a standard deviation of $\pm 25\%$, allowing us to obtain a distribution of expected predator diets as a function of prey mass. From this relationship, we then evaluated the expected predator mass for a given prey mass range to obtain $E\{M_P\}$ (Fig. 4b, main text), demonstrating the allometric relationship of $E\{M_P\} = 9.76 \times 10^3 M_C^{0.21}$, where we used the output of 100 independent replicates to robustly estimate the best fit. We emphasize that this relationship only pertains to large-bodied predators and prey $> 10^5 \text{ g}$. Alterations to and variations from this relationship are explored in the main text.

As explored in the main text, the empirically-measured PPMR for large-bodied mammals results in a threshold body size for herbivore consumers M_C^\dagger . This size marks the point where the predator population, with a body mass derived from the PPMR, cannot sustain its own growth from the predated herbivore population, thereby driving the herbivore population to extinction. The size at which M_C^\dagger occurs is both dependent on the nature of the PPMR, as well as predator specialization w . As w decreases such that the predator supports only a fraction of its growth from predation on the herbivore consumer, M_C^\dagger increases (Fig. S3).

By allowing the PPMR to vary as

$$E\{M_P\} = v_0(1 + \chi_{\text{int}})M_C^{v_1(1 + \chi_{\text{slope}})}, \quad (\text{S22})$$

where the proportional changes in the PPMR intercept and slope are given by χ_{int} and $\chi_{\text{slope}} \in (-0.99, 2)$, so does the threshold herbivore body mass M_C^\dagger and, by extension, the related threshold predator body mass M_P^\dagger . From Fig. 4d (main text), we observe that changing the intercept and slope of the PPMR has a large influence on M_C^\dagger and M_P^\dagger . Across this range of potential PPMR relationships, we highlight those values for the intercept and slope of the PPMR that permit megatrophic interactions, where both megapredators subsist on megaherbivores at the threshold body mass (highlighted region in Fig. 4d, main text). Fig. S4 shows the relationship between megapredator and megaherbivore body masses highlighted within this region. Allowing both the PPMR to vary and assuming the megapredator is a generalist ($w = 0.37$) rather than a specialist enables much larger body sizes for megaherbivores and their associated megapredators (Fig. S5).

SUPPLEMENTARY APPENDIX IV. DERIVATION OF HARVESTING MORTALITY

We first determined the harvest rate $h = h^\dagger$ required to drive an herbivore population to extinction, thereby satisfying the condition $C^*(M_C|h) = 0$ as a function of herbivore body mass M_C . This extinction-inducing harvest rate, itself now a function of consumer body mass $h^\dagger(M_C)$, defines the rate at which the population must be harvested to drive the steady state to zero. To compare this rate against measures of harvest both in nature and predicted from other mathematical or computational treatments of harvest-induced extinction, we calculated the harvest pressure ψ^\dagger , which we defined as the number of herbivore individuals per area harvested at this rate to reduce the population to some proportion ϵ of its steady state. This harvest pressure is thus defined by some number of individuals harvested per year over a certain number of years to reduce the population from C^* to its post-harvest density ϵC^* .

To calculate harvest pressure, we first assume that at the steady state, harvest is occurring on a shorter-than-generational timescale. For megaherbivores such as elephants, a generation is ca. 25 years (REF), and for harvest pressures that must be applied beyond this period of time, we would expect population growth to counter the negative effects of harvest. Assuming harvest-only change, we simplify the dynamics to

$$\frac{d}{dt}C = -h^\dagger(M_C)C, \quad (\text{S23})$$

where the time to reduce C^* to ϵC^* is

$$\begin{aligned} C(t) &= C_0 e^{-h^\dagger(M_C)t}, \\ \epsilon C^* &= C^* e^{-h^\dagger(M_C)t} \\ t_\epsilon &= -\frac{\log(\epsilon)}{h^\dagger(M_C)}. \end{aligned} \quad (\text{S24})$$

We note that for elephant-sized herbivores and larger, $t_\epsilon \leq 23$ years [76]. While the time required to harvest the population to ϵC^* is only just approaching generational timescales, it should be treated as a minimum t_ϵ given the effects of population growth will prolong the imposed harvest effort. Harvest pressure is then calculated as

$$\psi^\dagger = \frac{C^*(1-\epsilon)}{M_C t_\epsilon} c_0 = -h^\dagger(M_C) \frac{C^*(1-\epsilon)}{M_C \log(\epsilon)} c_0 \quad (\text{S25})$$

where the constant c_0 denotes the conversion from $\text{inds}/\text{m}^2/\text{second}$ to $\text{inds}/A_{\text{CA}}/\text{year}$, where $A_{\text{CA}} = 4.24 \times 10^{11} \text{ m}^2$ is the arbitrarily-chosen area of California. This conversion is particularly important for evaluating other harvest measures from the historical record and estimates from independent models and simulations for extinct species. As described in the main text, the extinction-inducing harvest pressure is calculated to be $4.3 \times 10^3 \text{ inds}/\text{yr}/A_{\text{CA}}$ for an elephant-sized organism of $M_C = 2.5 \times 10^6 \text{ g}$ (see Fig 5, main text).

Harvest pressure on Pleistocene mammoths We compare our measure of harvest pressure to that calculated for mammoths (*Mammuthus primigenius*) in Fordham et al. [61]. Because Fordham et al. employ a much more complex and detailed assessment of the effects of harvest specifically for mammoths over a spatially explicit landscape, we must make a few simplifications in order to derive a comparable estimate. First, the harvest interaction between mammoth populations and humans is modeled as a type 2 functional response, where, again isolating population-level effects to that of harvest we obtain

$$\frac{d}{dt}C = -\frac{sNFC}{G + \frac{C}{C_{\text{max}} M_C}}, \quad (\text{S26})$$

where N is the normalized human population density maximized at unity, the constant $s = 7.884 \times 10^{-8}$ generations/second (where a generation is 25 years), F represents the effectiveness of human hunting, ranging from $(0.01, 0.34)$, $C_{\text{max}} = 1.875 \times 10^{-6} \text{ g/m}^2$ is the maximum mammoth population density (converted from the average degree-by-degree grid cells in Siberia), $G = 0.4$ is the half-saturation constant, and $M_C = 2.5 \times 10^6 \text{ grams}$.

Solving for the time required to reduce the population to ϵC^* , we obtain

$$t_\epsilon^{\text{mammoth}} = \frac{C^* - C_{\text{max}} G M_C \log \left[C^* \exp \left(\frac{C^* \epsilon}{C_{\text{max}} G M_C} \right) \epsilon \right]}{s C_{\text{max}} F M_C N}. \quad (\text{S27})$$

We then calculate the harvest pressure as

$$\psi^{\text{mammoth}} = c_0 \frac{s C_{\text{max}} F N (C^* - C^* \epsilon)}{C^* - C_{\text{max}} G M_C \log \left[C^* \exp \left(\frac{C^* \epsilon}{C_{\text{max}} G M_C} \right) \epsilon \right]}, \quad (\text{S28})$$

where the constant c_0 again denotes the conversion from $\text{inds}/\text{m}^2/\text{second}$ to $\text{inds}/A_{\text{CA}}/\text{year}$, where A_{CA} is the arbitrarily-chosen area of California. Given a range in $F \in (0.01, 0.35)$ and $N \in (0.01, 1)$, we obtain a distribution of values for mammoth harvest pressure with a median value of $1.24 \times 10^4 \text{ inds}/\text{yr}/A_{\text{CA}}$ over the course of 9.8 years. The bounds of the estimated range from $5 \times 10^4 \text{ inds}/\text{yr}/A_{\text{CA}}$ over the course of 2 years to $5 \times 10^2 \text{ inds}/\text{yr}/A_{\text{CA}}$ over the course of ca. 200 years (the range is plotted as the vertical black line in Fig. 5, main text). Again we emphasize that these calculations of harvest pressure are derived from an extinction timescale that should be viewed as a minimum estimate given that we do not account for demographic rebound.

Harvest pressure on Pleistocene *Diprotodon* The harvest rate needed to collapse *Diprotodon* populations was calculated by Bradshaw et al. [13], where a harvest pressure of between 400-500 $\text{inds}/\text{year}/\text{area}$ of Australia was sufficient. Translating this to the area of California, we obtain between 678 to 848 $\text{inds}/\text{yr}/A_{\text{CA}}$, with a mean of 763.2 $\text{inds}/\text{yr}/A_{\text{CA}}$.

Harvest pressure on historical elephants *Loxodonta africana* Elephant harvest rates are estimated from historical documentation of the ivory trade detailed in Milner-Gulland & Beddington [62]. While the trade volume oscillates with changes in technology, access to habitats within Africa, and the feedbacks of trade on elephant population size, we compare our results against estimates taken at two points in time: early in the ivory trade (1810), and late in the ivory trade (1987). From [62] we assume that each elephant killed contributes 1.88 tusks, and that tusk mass begins at 15 kg per tusk early in trade to 5 kg per tusk in later years. While the area from which elephants were harvested is largely unknown, we assume the area harvested is that assessed to be suitable elephant habitat in sub-Saharan Africa, estimated at $3.22 \times 10^{12} \text{ m}^2$ [77]. From rates of ca. $1 \times 10^5 \text{ kg/yr}$ of ivory harvested in 1810 to ca. $9.7 \times 10^5 \text{ kg/yr}$ of ivory harvested in 1987, normalized to habitat area and converted to the area of California, we obtain estimates of ca. 467 inds/yr/ A_{CA} in 1810 to ca. $1.33 \times 10^4 \text{ inds/yr}/A_{\text{CA}}$ in 1987 (see Fig. 5, main text).

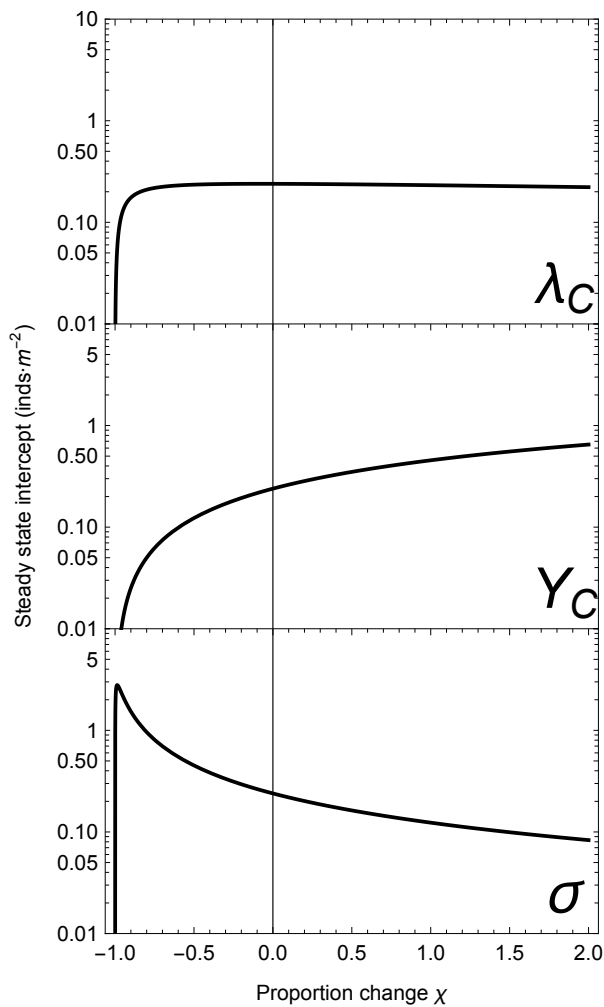


Figure S1: The effects of changes to metabolic parameters on the prediction of the mass-density relationship.

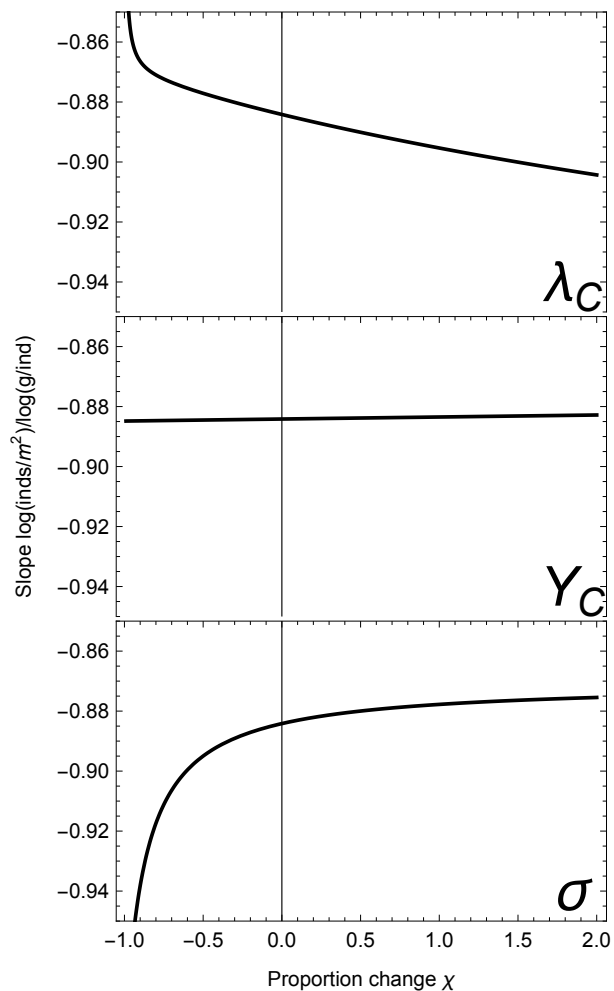


Figure S2: The effects of changes to metabolic parameters on the prediction of the mass-density relationship.

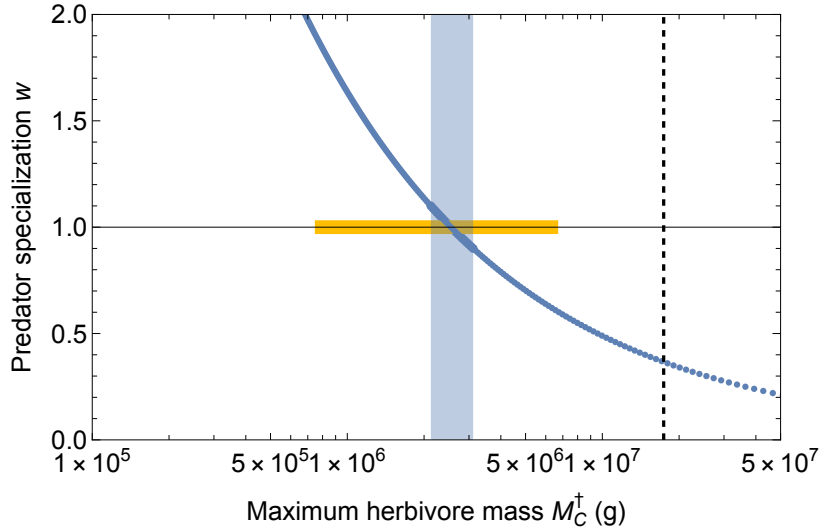


Figure S3: The effect of changing the reliance of predator growth w on the single herbivore consumer population. If $w = 1$, the predator solely relies on the herbivore consumer. If $0 < w < 1$, the predator relies on the herbivore population to support a fraction of its growth. If $w > 1$, the predator is removing more biomass than is necessary to support its growth. Blue region denotes herbivore threshold mass range characterizing $w = 1 \pm 0.1$. Yellow line denotes the mass range of contemporary elephants. Vertical dashed line denotes the size of the largest terrestrial mammal (*Deinotherium* at ca. 1.74×10^7 , corresponding to $w = 0.37$, such that a predator is supporting a little more than $1/3$ of its growth from the herbivore consumer.

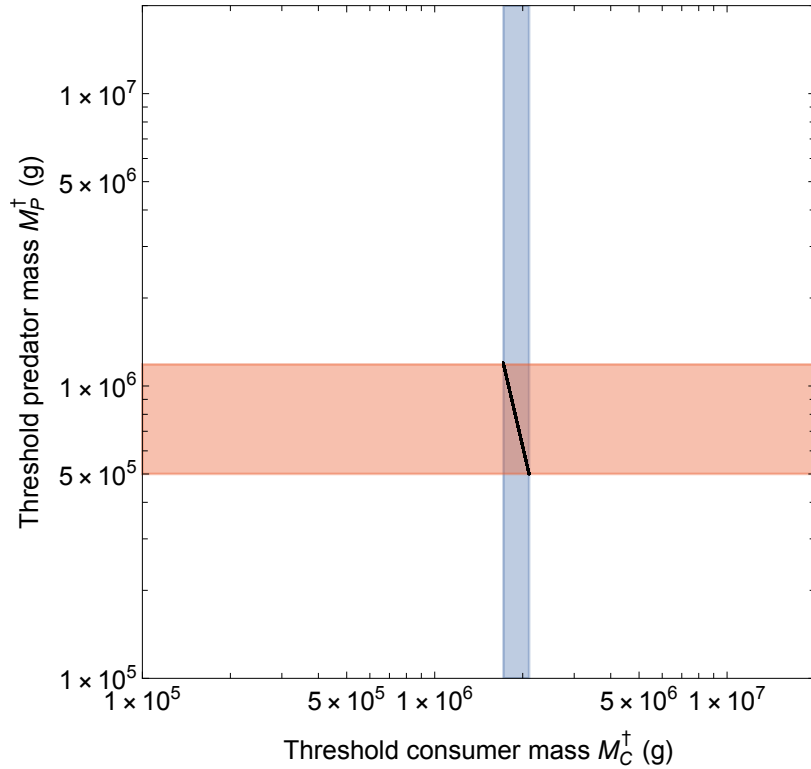


Figure S4: Mass ranges corresponding to feasible megatrophic interactions (where herbivore and predator threshold masses are $> 5 \times 10^5$ g) across variations to the assumed predator-prey mass ratio (PPMR), demarcated by the white bands in Fig. 4c,d, and under the assumption specialist predation ($w = 1$).

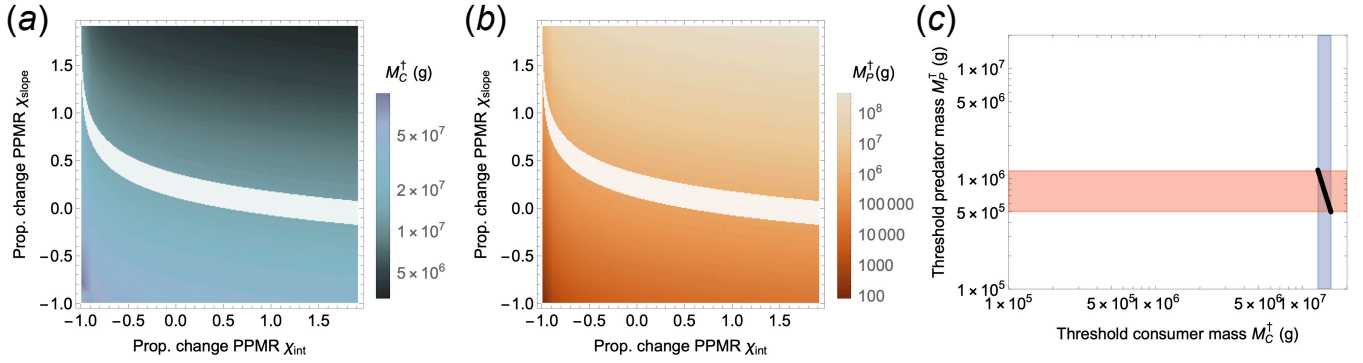


Figure S5: The effects of predator generalization ($w = 0.37$) on a) threshold herbivore mass M_C^\dagger and b) threshold predator mass M_P^\dagger across variable PPMRs, where $E\{M_P\} = v_0(1 + \chi_{\text{int}})M_C^{v_1(1+\chi_{\text{slope}})}$ and both χ_{int} and $\chi_{\text{slope}} \in (-0.99, 2)$, and $v_0 = 9.76 \times 10^3$ and $v_1 = 0.21$ are set as in the main text. White bands denote regions of χ_{int} and χ_{slope} where megatrophic interactions are feasible (i.e. both predator and herbivore threshold masses are $> 5 \times 10^5$ g). c) Mass ranges corresponding to feasible megatrophic interactions in the white bands in (a) and (b).

[1] DeAngelis D. 1980 Energy flow, nutrient cycling, and ecosystem resilience. *Ecology* **61**, 764–771.

[2] Yodzis P, Innes S. 1992 Body Size and Consumer-Resource Dynamics. *Am. Nat.* **139**, 1151–1175.

[3] Hou C, Zuo W, Moses ME, Woodruff WH, Brown JH, West GB. 2008 Energy Uptake and Allocation During Ontogeny. *Science* **322**, 736–739.

[4] Lindstedt SL, Schaeffer PJ. 2002 Use of allometry in predicting anatomical and physiological parameters of mammals.. *Lab. Anim.* **36**, 1–19.

[5] West GB, Brown JH, Enquist BJ. 2001 A general model for ontogenetic growth. *Nature* **413**, 628–631.

[6] Hennemann WW. 1983 Relationship among body mass, metabolic rate and the intrinsic rate of natural increase in mammals. *Oecologia* **56**, 104–108.

[7] West GB, Woodruff WH, Brown JH. 2002 Allometric scaling of metabolic rate from molecules and mitochondria to cells and mammals.. *Proc. Natl. Acad. Sci. USA* **99 Suppl 1**, 2473–2478.

[8] Kempes CP, Dutkiewicz S, Follows MJ. 2012 Growth, metabolic partitioning, and the size of microorganisms.. *PNAS* **109**, 495–500.

[9] Yeakel JD, Kempes CP, Redner S. 2018 Dynamics of starvation and recovery predict extinction risk and both Damuth's law and Cope's rule. *Nature communications* **9**, 1–10.

[10] Bhat U, Kempes CP, Yeakel JD. 2020 Scaling the risk landscape drives optimal life-history strategies and the evolution of grazing. *Proceedings of the National Academy of Sciences* **117**, 1580–1586.

[11] Alroy J. 2001 A multispecies overkill simulation of the end-Pleistocene megafaunal mass extinction. *Science* **292**, 1893–1896.

[12] Brook BW, Sodhi NS, Bradshaw CJ. 2008 Synergies among extinction drivers under global change. *Trends in ecology & evolution* **23**, 453–460.

[13] Bradshaw CJ, Johnson CN, Llewelyn J, Weisbecker V, Strona G, Saltré F. 2021 Relative demographic susceptibility does not explain the extinction chronology of Sahul's megafauna. *Elife* **10**, e63870.

[14] Murdoch WW, Briggs CJ, Nisbet RM. 2003 *Consumer-resource Dynamics*. Monographs in population biology. Princeton University Press.

[15] Calder III WA. 1983 An allometric approach to population cycles of mammals. *J. Theor. Biol.* **100**, 275–282.

[16] Robert A, Chantepie S, Pavard S, Sarrazin F, Teplitsky C. 2015 Actuarial senescence can increase the risk of extinction of mammal populations. *Ecological Applications* **25**, 116–124.

[17] Alonso SH. 2002 State-dependent habitat selection games between predators and prey: the importance of behavioural interactions and expected lifetime reproductive success. *Evol. Ecol. Res.* **4**, 759–778.

[18] Dunne JA, Maschner H, Betts MW, Huntly N, Russell R, Williams RJ, Wood SA. 2016 The roles and impacts of human hunter-gatherers in North Pacific marine food webs. *Sci. Rep.* **6**, 1–9.

[19] Damuth J. 1987 Interspecific allometry of population density in mammals and other animals: the independence of body mass and population energy-use. *Biol. J. Linn. Soc.* **31**, 193–246.

[20] DeLong JP, Vasseur DA. 2012 Size-density scaling in protists and the links between consumer–resource interaction parameters. *J. Anim. Ecol.* **81**, 1193–1201.

[21] Savage VM, Gillooly JF, Brown JH, West GB, Charnov EL. 2004 Effects of Body Size and Temperature on Population Growth. <http://dx.doi.org.proxy.lib.sfu.ca/10.1086/679735> **163**, 429–441.

[22] Smith F, Boyer A, Brown J, Costa D. 2010 The Evolution of Maximum Body Size of Terrestrial Mammals. *Science*.

[23] DeLong JP, Okie JG, Moses ME, Sibly RM, Brown JH. 2010 Shifts in metabolic scaling, production, and efficiency across major evolutionary transitions of life.. *PNAS* **107**, 12941–12945.

[24] Millar J, Hickling G. 1990 Fasting Endurance and the Evolution of Mammalian Body Size. *Funct. Ecol.* **4**, 5–12.

[25] Yeakel JD, Bhat U, Newsome SD. 2020 Caching in or falling back at the Sevilleta: the effects of body size and seasonal uncertainty on desert rodent foraging. *The American Naturalist* **196**, 241–256.

[26] Schubert KA, Boerema AS, Vaanholt LM, de Boer SF, Strijkstra AM, Daan S. 2010 Daily torpor in mice: high foraging costs trigger energy-saving hypothermia. *Biology letters* **6**, 132–135.

[27] Geiser F. 1998 Evolution of daily torpor and hibernation in birds and mammals: importance of body size. *Clinical and experimental pharmacology and physiology* **25**, 736–740.

[28] Smith C, Reichman O. 1984 The evolution of food caching by birds and mammals. *Annual Review of Ecology and Systematics* **15**, 329–351.

[29] Carbone C, Gittleman JL. 2002 A common rule for the scaling of carnivore density. *Science* **295**, 2273–2276.

[30] Sinclair ARE, Mduma S, Brashares JS. 2003 Patterns of predation in a diverse predator–prey system. *Nature* **425**, 288–290.

[31] Brose U, Cushing L, Berlow EL, Jonsson T. 2005 Body sizes of consumers and their resources. *Ecology*.

[32] Hatton IA, McCann KS, Fryxell JM, Davies TJ, Smerlak M, Sinclair ARE, Loreau M. 2015 The predator-prey power law: Biomass scaling across terrestrial and aquatic biomes.. *Science* **349**, aac6284–aac6284.

[33] Barnes C, Maxwell D, Reuman DC, Jennings S. 2010 Global patterns in predator–prey size relationships reveal size dependency of trophic transfer efficiency. *Ecology* **91**, 222–232.

[34] Rohr RP, Scherer H, Kehrli P, Mazza C, Bersier LF. 2010 Modeling food webs: Exploring unexplained structure using latent traits. *Am. Nat.* **176**, 170–177.

[35] Riede JO, Brose U, Ebenman B, Jacob U, Thompson R, Townsend CR, Jonsson T. 2011 Stepping in Elton's footprints: a general scaling model for body masses and trophic levels across ecosystems. *Ecology letters* **14**, 169–178.

[36] Yeakel JD, Pires MM, Rudolf L, Dominy NJ, Koch PL, Guimarães Jr PR, Gross T. 2014 Collapse of an ecological network in Ancient Egypt. *Proceedings of the National Academy of Sciences* **111**, 14472–14477.

[37] Pires MM, Koch PL, Fariña RA, de Aguiar MA, dos Reis SF, Guimarães Jr PR. 2015 Pleistocene megafaunal interaction networks became more vulnerable after human

arrival. *Proceedings of the Royal Society B: Biological Sciences* **282**, 20151367.

[38] Nakazawa T. 2017 Individual interaction data are required in community ecology: a conceptual review of the predator–prey mass ratio and more. *Ecological Research* **32**, 5–12.

[39] Hayward MW, Kerley GI. 2005 Prey preferences of the lion (*Panthera leo*). *Journal of zoology* **267**, 309–322.

[40] Hayward M. 2006 Prey preferences of the spotted hyaena (*Crocuta crocuta*) and degree of dietary overlap with the lion (*Panthera leo*). *J. Zoology* **270**, 606–614.

[41] Hayward M, Henschel P, O'Brien J, Hofmeyr M, Balme G, Kerley GI. 2006a Prey preferences of the leopard (*Panthera pardus*). *Journal of Zoology* **270**, 298–313.

[42] Hayward MW, O'Brien J, Hofmeyr M, Kerley GI. 2006b Prey preferences of the African wild dog *Lycaon pictus* (Canidae: Carnivora): ecological requirements for conservation. *Journal of Mammalogy* **87**, 1122–1131.

[43] Hayward M, Hofmeyr M, O'Brien J, Kerley GI. 2006c Prey preferences of the cheetah (*Acinonyx jubatus*) (Felidae: Carnivora): morphological limitations or the need to capture rapidly consumable prey before kleptoparasites arrive?. *Journal of Zoology* **270**, 615–627.

[44] Hayward MW, Kerley G. 2008 Prey preferences and dietary overlap amongst Africa's large predators. *S. African J. Wildl. Res.* **38**, 93–108.

[45] Cruz LR, Muylaert RL, Galetti M, Pires MM. 2022 The geography of diet variation in Neotropical Carnivora. *Mammal Review* **52**, 112–128.

[46] Cruz LR, Pires MM. 2022 Body mass ratios determine dietary patterns and help predicting predator–prey interactions of Neotropical Carnivora. *Mammal Research*.

[47] Gross T, Rudolf L, Levin SA, Dieckmann U. 2009 Generalized models reveal stabilizing factors in food webs. *Science* **325**, 747–750.

[48] Kay CE. 2002 False gods, ecological myths, and biological reality. *Wilderness and political ecology: aboriginal influences and the original state of nature*. University of Utah Press, Salt Lake City pp. 238–261.

[49] Ripple WJ, Van Valkenburgh B. 2010 Linking top-down forces to the Pleistocene megafaunal extinctions. *BioScience* **60**, 516–526.

[50] Burness GP, Diamond J, Flannery T. 2001 Dinosaurs, dragons, and dwarfs: the evolution of maximal body size. *Proceedings of the National Academy of Sciences* **98**, 14518–14523.

[51] Sorkin B. 2008 A biomechanical constraint on body mass in terrestrial mammalian predators. *Lethaia* **41**, 333–347.

[52] Carbone C, Teacher A, Rowcliffe JM. 2007 The Costs of Carnivory. *PLoS Biol* **5**, e22.

[53] Farlow JO. 1993 On the rareness of big, fierce animals; speculations about the body sizes, population densities, and geographic ranges of predatory mammals and large carnivorous dinosaurs. *American Journal of Science* **293**, 167.

[54] van Valkenburgh B, Wang X, Damuth J. 2004 Cope's rule, hypercarnivory, and extinction in North American canids. *Science* **306**, 101.

[55] Brook BW, Bowman DMJS. 2005 One equation fits overkill: why allometry underpins both prehistoric and modern body size-biased extinctions. *Population Ecology* **47**, 137–141.

[56] Churchill SE. 1993 Weapon technology, prey size selection, and hunting methods in modern hunter-gatherers: implications for hunting in the Palaeolithic and Mesolithic. *Archeological Papers of the American Anthropological Association* **4**, 11–24.

[57] Ugan A. 2005 Does size matter? Body size, mass collecting, and their implications for understanding prehistoric foraging behavior. *American Antiquity* **70**, 75–89.

[58] Prates L, Rivero D, Perez SI. 2022 Changes in Projectile design and size of prey reveals the role of Fishtail points in megafauna hunting in South America. *Preprint: https://doi.org/10.21203/rs.3.rs-1569375/v1*.

[59] Smith FA, Elliott Smith RE, Lyons SK, Payne JL. 2018 Body size downgrading of mammals over the late Quaternary.. *Science* **360**, 310–313.

[60] Enquist BJ, Abraham AJ, Harfoot MB, Malhi Y, Doughty CE. 2020 The megabiota are disproportionately important for biosphere functioning. *Nature communications* **11**, 1–11.

[61] Fordham DA, Brown SC, Akçakaya HR, Brook BW, Haythorne S, Manica A, Shoemaker KT, Austin JJ, Blonder B, Pilowsky J et al.. 2022 Process-explicit models reveal pathway to extinction for woolly mammoth using pattern-oriented validation. *Ecology letters* **25**, 125–137.

[62] Milner-Gulland E, Beddington J. 1993 The exploitation of elephants for the ivory trade: an historical perspective. *Proceedings of the Royal Society of London. Series B: Biological Sciences* **252**, 29–37.

[63] Horton DR, Wright RV. 1981 Cuts on Lancefield bones: carnivorous *Thylacoleo*, not humans, the cause. *Archaeology in Oceania* **16**, 73–80.

[64] Wroe S, Myers T, Wells R, Gillespie A. 1999 Estimating the weight of the Pleistocene marsupial lion, *Thylacoleo carnifex* (Thylacoleonidae: Marsupialia): implications for the ecomorphology of a marsupial super-predator and hypotheses of impoverishment of Australian marsupial carnivore faunas. *Australian Journal of Zoology* **47**, 489–498.

[65] Webb S. 2009 Late Quaternary distribution and biogeography of the southern Lake Eyre basin (SLEB) megafauna, South Australia. *Boreas* **38**, 25–38.

[66] Cardillo M, Mace GM, Jones KE, Bielby J, Bininda-Emonds ORP, Sechrest W, Orme CDL, Purvis A. 2005 Multiple causes of high extinction risk in large mammal species. *Science* **309**, 1239–1241.

[67] Johnson CN. 2002 Determinants of loss of mammal species during the Late Quaternary 'megafauna' extinctions: life history and ecology, but not body size. *Proceedings of the Royal Society of London. Series B: Biological Sciences* **269**, 2221–2227.

[68] Estes JA, Terborgh J, Brashares JS, Power ME, Berger J, Bond WJ, Carpenter SR, Essington TE, Holt RD, Jackson JBC, Marquis RJ, Oksanen L, Oksanen T, Paine RT, Pikitch EK, Ripple WJ, Sandin SA, Scheffer M, Schoener TW, Shurin JB, Sinclair ARE, Soulé ME, Virtanen R, Wardle DA. 2011 Trophic downgrading of planet Earth. *Science* **333**, 301–306.

[69] Michaletz ST, Cheng D, Kerkhoff AJ, Enquist BJ. 2014 Convergence of terrestrial plant production across global climate gradients. *Nature* **512**, 39–43.

[70] De Jager NR, Drohan PJ, Miranda BM, Sturtevant BR, Stout SL, Royo AA, Gustafson EJ, Romanski MC. 2017 Simulating ungulate herbivory across forest landscapes: A browsing extension for LANDIS-II. *Ecological Modelling* **350**, 11–29.

[71] Pedersen RØ, Faurby S, Svenning JC. 2017 Shallow

size-density relations within mammal clades suggest greater intra-guild ecological impact of large-bodied species. *J. Anim. Ecol.* **86**, 1205–1213.

[72] Koch PL, Barnosky A. 2006 Late Quaternary extinctions: state of the debate. *Annu. Rev. Ecol. Evol. Syst.* **37**, 215–250.

[73] Muñoz-García, Agustí and Williams, Joseph B.. 2005 Basal metabolic rate in carnivores is associated with diet after controlling for phylogeny. *Physiological and Biochemical Zoology* **78**, 1039–1056. PMID: 16228943.

[74] Prange HD, Anderson JF, Rahn H. 1979 Scaling of skeletal mass to body mass in birds and mammals. *The American Naturalist* **113**, 103–122.

[75] Merrill A, Watt B. 1973 Part 2: digestibility and available energy of foods. *Energy value of foods: basis and derivation. Agriculture handbook No 74*, 8–24.

[76] Wittemyer G, Daballen D, Douglas-Hamilton I. 2013 Comparative demography of an at-risk African elephant population. *PLoS one* **8**, e53726.

[77] Thouless C, Dublin HT, Blanc J, Skinner D, Daniel T, Taylor R, Maisels F, Frederick H, Bouché P. 2016 African elephant status report 2016. *An update from the African Elephant Database*.